Top-Coat Dewetting for the Highly Ordered Lateral Alignment of Block Copolymer Microdomains in Thin Films

*Eunkyoung Yoon, Eunjin Kim, Daeheum Kim, and Jeong Gon Son**

Extremely straight and laterally aligned cylindrical microdomains of block copolymer (BCP) films have been prepared by simply covering the BCP films with a top coat and dewetting the latter via thermal annealing to generate shear flow in the BCP underlayer. The polystyrene-*block*-polydimethylsiloxane microdomains are perfectly aligned with sunburst direction along the polyvinyl alcohol top-coat dewetting front from the nucleation point to the end of the dewetting front. This alignment is at least 150 μm long and the aspect ratio is higher than 15 000:1. Studying the morphologies obtained as a function of top-coat and BCP film thickness at various annealing temperatures, highly ordered BCP patterns are obtained for a wide range of shear rates, while higher (but not the highest) temperatures and thicker BCP films lead to more ordered microdomain patterns, because of increased polymer mobility and a reduced surface/interface effect. An imprinting process is also introduced to pattern top coats, which then provide selective control of the dewetting direction so that unidirectionally aligned BCP patterns can be created in specific areas.

1. Introduction

Self-assembly of block copolymers (BCPs) can be spontaneously phase-separated within copolymer chains and produce nanoscale periodic patterns five to several hundred nanometers in length.[1,2] Thus, BCP thin films have studied intensively as an advanced lithographic tool to realize cost-effective sub-20 nm device fabrication method.[3–6] However, BCP self-assembly is generally limited to the formation of randomly oriented fingerprint patterns, whereas better control of the orientation and directional alignment of microdomains would be desirable to form the more complex structures useful in devices. To achieve highly ordered and directionally controlled BCP patterns, the combination of the BCP self-assembly based bottom-up processes and conventional top-down approaches, such as photolithography[7–12] or e-beam lithography,[13–16] has been investigated. Among these, graphoepitaxy, which involves guiding BCP patterns with a topographical template,[7–14] and chemoepitaxy, where the patterns are guided on chemical stripes with commensurable pattern periods,[15–17] are generating a lot of interest in the semiconductor and advanced lithography fields.[18] However, the narrow commensurability conditions between BCPs and the top-down patterns, the complex patterning processes, line edge roughness problems, and the subtle interface neutralization conditions of the substrate are also issues that should be resolved to realize less defected and device-applicable patterns.

The directional alignment of BCP microdomains without the top-down process has also been studied, notably via alignment in coffee-stain microstructures,[19] on saw-tooth patterns,[20] in magnetic fields,[21,22] and using shear flow.[23–29] Among these approaches, shear alignment has long been used in bulk- or thick-film block copolymer systems because the BCP microdomains readily orient parallel to the flow direction leading to the formation of macroscopic near-single-crystal textures.[23,24] On the other hand, the use of shear alignment for thin films is more complicated, with difficulties in achieving uniform shear and conformal contact, and avoiding delamination from the substrate. Angelescu et al. introduced elastomeric polydimethylsiloxane (PDMS) pads on BCP thin films to resolve these issues and realized unidirectionally aligned single-layer cylindrical arrays of BCP microdomains over a large area,[25] and Singh et al. further improved using cold zone annealing.[26] Soft shearing with solvent annealing have also been used to align BCP microdomains.[28,29] However, this shear alignment with pad displacement only produces a unidirectional alignment across the entire shear area, not the multidirectional or selective alignment at the specific part in a single unit. For the multidirectional alignment, flowing nonsolvent liquid through a microfluidic multidirectional channel on BCP films has been shown to induce the directional alignment of microdomains,[27] but inevitably, this approach is prone to fluid leakage and BCP film sweeping.

The concept of a top coat can be a solution for the directional alignment with controllable surface/interfacial tension of BCP films. Recently, the top coat has been used for production of perpendicularly ordered BCP microdomains with a high aspect

E. Yoon, E. Kim, Dr. J. G. Son
Photo-Electronic Hybrids Research Center
Korea Institute of Science and Technology (KIST)
Seoul 136-791, Korea
E-mail: jgson@kist.re.kr
E. Yoon, Prof. D. Kim
Department of Chemical Engineering
Kwangwoon University
Seoul 139-701, Korea

DOI: 10.1002/adfm.201403046

ratio, whereby the top surface energy difference between two blocks is neutralized.[30–32] Our group also demonstrated the fully perpendicular orientation of polystyrene-*block*-polydimethylsiloxane (PS-*b*-PDMS) cylindrical microdomains, which has one of the largest surface energy differences between the two blocks, using a polyvinyl alcohol (PVA) top coat and solvent annealing.[33] However, perpendicular orientation in the PVA/PS-*b*-PDMS bilayer system was not achieved with conventional high temperature thermal annealing, dewetting of the hydrophilic top coat on the BCP film was obtained instead. Dewetting involves the rupture of a thin liquid film on the substrate leading to the formation of droplets.[34] Indeed, during the dewetting process, the rim of the dewetting top coat moves to the undewetted region with a plug flow behavior that can exert a steady shear force on the underlying BCP film.

In this paper, using this top-coat dewetting phenomenon at high temperatures, we demonstrate the formation of extremely straight and laterally ordered 10 nm-wide PS-*b*-PDMS cylindrical microdomains in thin films. This top-coat dewetting of the PVA/BCP bilayer films produces straight cylinders arranged radially in a regular sunburst-type pattern from the nucleation point to the end of dewetting front, at least 150 μm in length and 15 000:1 in aspect ratio. We examined the microdomain morphologies of BCP films as a function of BCP films and top coat thickness, and annealing temperature. Highly ordered BCP patterns were obtained for a wide range of shear rates, but diminished surface/interface effects at thicker BCP films and higher polymer mobility lead to improved microdomain ordering. To explore the possibility of controlled multidirectional alignment in specific areas, top-coat dewetting was combined with imprinting to form topographical patterns on the top coat, whereby microdomains strongly aligned in the direction normal to the imprinted line-space patterns were produced in 80 μm wide trenches.

2. Results and Discussion

The dewetting of the PVA top coat on PS-*b*-PDMS thin films leads to the formation of highly aligned BCP microdomains in sunburst-type patterns under thermal annealing, as illustrated in **Figure 1**. Dewetting usually occurs when a polymeric film is energetically unstable on the substrate and is sufficiently

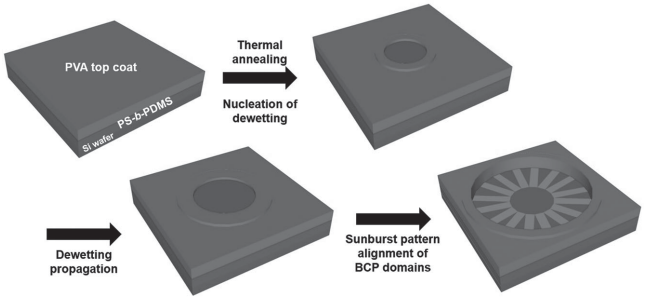

Figure 1. Schematic illustration of the production of highly aligned sunburst-patterned block copolymer (BCP) microdomains by top-coat dewetting of PS-*b*-PDMS thin films at annealing temperatures above the glass transition temperature.

mobile at temperatures above the glass transition temperature. A negative spreading coefficient, $S = \gamma_B - \gamma_A - \gamma_{AB}$, where γ_A, γ_B, and γ_{AB} are, respectively, the surface tensions of the upper film and the substrate, and the interfacial tension of the film–substrate interfaces, indicates that dewetting will occur.[34] In this work, we prepared the bilayer film using 40% hydrolyzed PVA (PVA40) as a top coat and 16k cylindrical PS-*b*-PDMS block copolymer film as an underlayer. Since the surface tensions of PVA40, PS, and PDMS are 42.4 mN m^{-1}, 40.7 mN m^{-1}, and 20.4 mN m^{-1}, and the interfacial tensions of PVA40-PS and PVA40-PDMS are 4.67 mN m^{-1} and 14.7 mN m^{-1}, respectively,[33] this bilayer system has a negative spreading coefficient with either the PS or PDMS substrate and top-coat dewetting should therefore occur at sufficiently high temperatures. However, no dewetting was observed during the 2 h of thermal annealing for the PS-*b*-PDMS films on pristine Si wafer because of its high surface tension (≈55.6 mN m^{-1}).

During the early stages of top-coat dewetting, surface instabilities lead to the nucleation of holes at certain points on the BCP film, which then grow radially over time. The annealing temperature was typically 180 °C, which is much higher than the glass transition temperature (T_g) of PVA40 (67 °C, confirmed by differential scanning calorimetry (DSC) in Figure S1, Supporting Information) and of PS-*b*-PDMS BCP ($T_{g,PS} \approx 100$ °C and $T_{g,PDMS} \approx -123$ °C).[35] Thus, during thermal annealing, dewetting of the top coat and self-assembly of the BCP occur simultaneously. In a conventional liquid/liquid dewetting system, the dewetted rim of the top coat advances via plug flow producing a steady shear flow in the thin liquid underlayer between this rim and the substrate.[34] Therefore, steady dewetting-assisted shear flow of the BCP film can align the cylindrical PS-*b*-PDMS microdomains along the direction of rim propagation, resulting in the formation within the dewetted holes of highly aligned BCP microdomains in sunburst-type patterns over several hundreds of micrometers.

Figure 2a shows an optical microscopy (OM) image of a dewetted PVA top coat (300 nm area) on a 150 nm thick PS-*b*-PDMS film after 2 h of annealing at 180 °C. The top coat was fully dewetted within several minutes to an hour, with the formation of cellular patterns and droplets. The average hole diameter was approximately 400 μm. Different colored areas are observed in the BCP films within the dewetted holes, indicating quantized differences in thickness originating from the parallel orientation of microdomains with incommensurable film thicknesses (in other words, to hole/island structures). Using scanning electron microscopy (SEM), we investigated the morphology of the BCP film in specific areas taken in eight directions ±50 μm away from the dewetting nucleation point (Figure 2j), as shown in Figure 2b–i. 10 nm wide BCP cylindrical microdomains are uniformly aligned in a single direction over a 5 μm × 5 μm in each area and the cylinder alignments of each area in eight directions are entirely heading for the nucleation point. Orientational color maps obtained from the SEM images in the insets of Figure 2b–i show different monotone colors for each area, demonstrating visually the arrangement of the cylinders at specific angles according to the sunburst pattern. This directional alignment formed whole thickness range of the films, which was confirmed by cross-section SEM image in the inset of Figure 2j. Randomly oriented parallel BCP

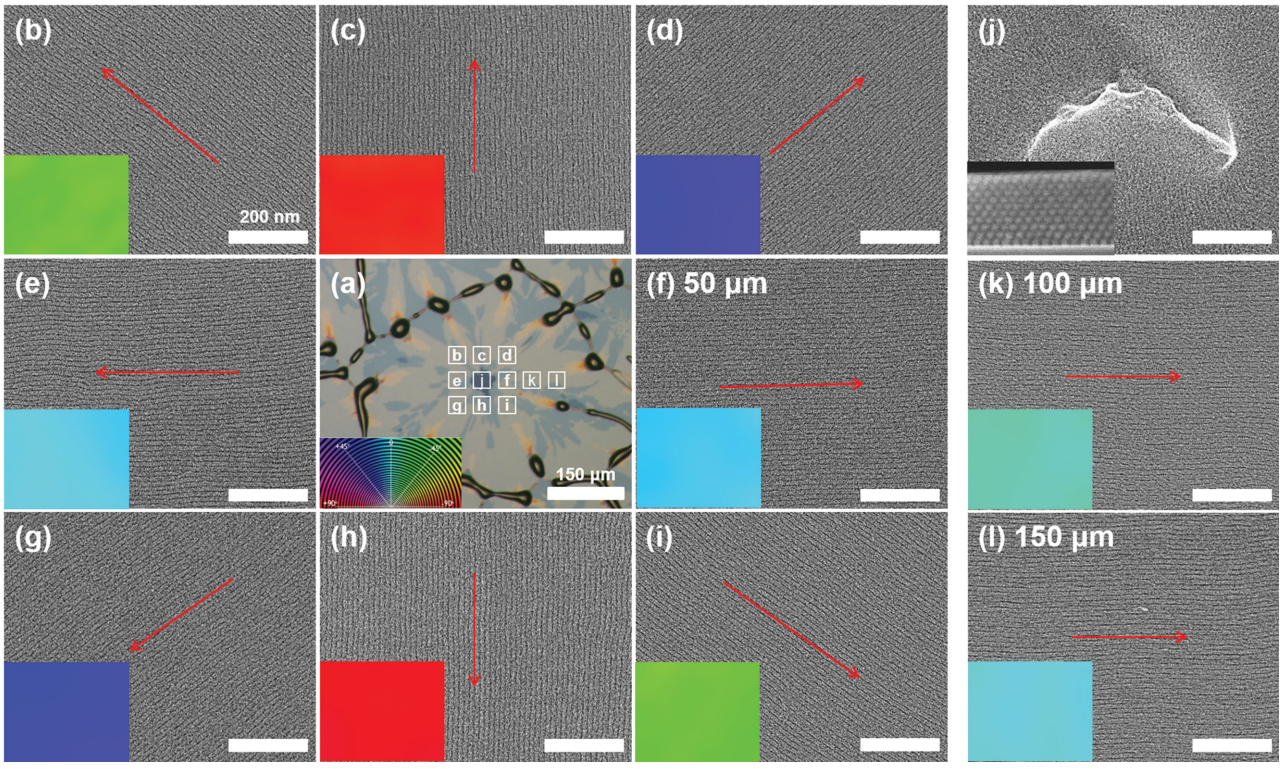

Figure 2. a) Optical images of a dewetted PVA top coat (300 nm thick) on a PS-*b*-PDMS film (150 nm thick) after thermal treatment at 180 °C for 2 h. b–i) Scanning electron images of block copolymer microdomains taken in eight regions 50 µm apart surrounding the dewetting nucleation point. j) Scanning electron image of the nucleation point on a block copolymer film after top-coat dewetting and (inset) cross-sectioned image of dewetted BCP films. Scanning electron images of block copolymer microdomains k) 100 µm and l) 150 µm away from the dewetting nucleation point. The insets show orientational color map images obtained from the corresponding images.

microdomain cylinders are observed in the region wetted by the PVA droplet.

We also examined the BCP morphologies 100 µm (Figure 2k) and 150 µm (Figure 2l) away from the nucleation point in the same direction as for Figure 2f. The images and the corresponding color maps reveal highly aligned BCP microdomains whose orientation is independent of the distance from the nucleation point. This result indicates that the directional alignment of 10 nm-wide line patterns proceeds from the nucleation point to the rim of dewetted top coat, over a distance of at least 150 µm and with an aspect ratio of 15 000:1. Furthermore, by controlling the direction of the top-coat dewetting front, the alignment of the BCP microdomains can be micromanaged in specific areas.

BCP film thicknesses are always critical in determining the orientation of the microdomains and their commensurability with the BCP domain period because of the conflict between the bulk properties of BCPs and top/bottom surface interface effects. Furthermore, BCP film thickness is directly related to the shear rate ($\gamma = \upsilon/h$, where υ is the velocity of the dewetting front and h is the thickness of the BCP underlayer). The effect of 50–500 nm-thick BCP films on the degree of orientational order of the BCP microdomains was examined for a single top coat thickness (300 nm) and annealing temperature (180 °C). As shown in the SEM images and the corresponding color maps of **Figure 3**a–f, directional but less ordered and wavy line patterns are obtained with 50 nm and 100 nm-thick films, while with 150 nm or thicker films the resulting line patterns are almost perfectly straight. To quantify the alignment of the BCP line patterns, we define an orientational order parameter (ψ)[36]

$$\psi = \langle \cos[2(\theta - \theta_0)] \rangle$$

where θ is the local orientational angle of the line and θ_0 is the angle of the dewetting front direction. The orientational order parameters calculated for the 50 nm, 100 nm, and ≥150 nm-thick films are ≈0.93, ≈0.96, and ≈0.975, respectively, the latter value being close to that obtained for perfectly straight line patterns (Figure 3g). Under these bilayer dewetting conditions, the dewetting front progressed at approximately 220 nm s^{-1}, as measured using an optical microscope equipped with a digital camera, while the calculated shear rates ranged from 4.4 s^{-1} to 0.44 s^{-1}. In contrast with previous studies of BCP shear alignment,[25,36,37] the aligning shear rates are more than one order of magnitude below the suggested threshold. Furthermore, thinner BCP films and higher shear rates lead to less ordered cylindrical patterns than those obtained with thicker films and less shearing. We think that this straight alignment of BCP films obtained even at relatively low shear rates is mainly due to the high mobility of low molecular weight PS-*b*-PDMS (M_w ≈16 kg mol^{-1}) BCP. The lower degree of alignment of the microdomains obtained with the thinner BCP films may also be the result of a substrate pinning effect that originates from the strong interaction between the BCP chains and the hydroxyl-terminated native oxide surface.[9,38]

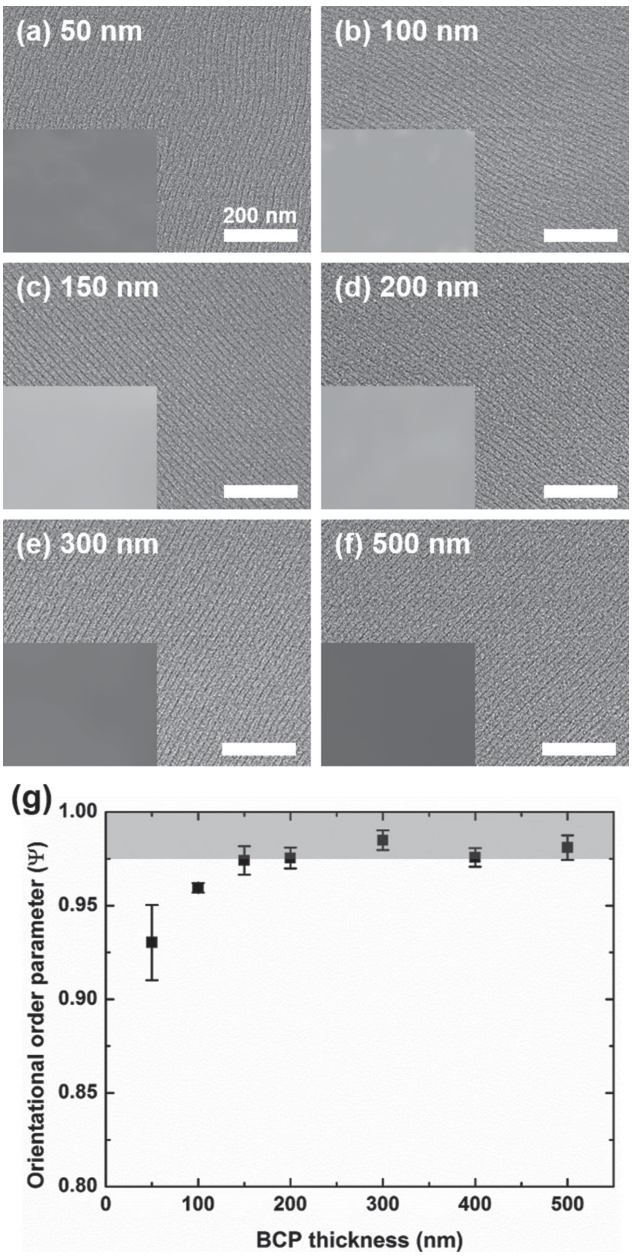

Figure 3. Scanning electron images of the block copolymer alignments obtained with a) 50 nm, b) 100 nm, c) 150 nm, d) 200 nm, e) 300 nm, and f) 500 nm-thick block copolymer films covered with a 300 nm-thick PVA top coat and annealed for 2 h at 180 °C. The insets show orientational color map images from the corresponding images. g) Orientational order parameters of the aligned microdomains as a function of block copolymer (BCP) film thickness.

The temperature of thermal annealing can affect not only the mobility and alignment of the BCP microdomains, but also the dewetting behavior of the top coat and the velocity of the dewetting front. **Figure 4** shows OM and SEM images of PVA/BCP (300/150 nm thick), bilayer films obtained after annealing for 2 h at different temperatures, as well as the orientational order parameters and dewetting velocities measured as a function of the annealing temperature. As the annealing temperature increases, so do the mobility the polymers in the bilayer films and the dewetting velocity. At 120 °C and 140 °C, slightly higher than the T_g of PS, because the BCP films are not sufficiently mobile and the dewetting velocity is also very low (≈10 nm s^{-1} and ≈45 nm s^{-1}, respectively), the BCP microdomains were not fully aligned along the shear direction. Higher annealing temperatures (160 °C and 180 °C) ensure that the BCP microdomains are sufficiently mobile and induce rapid top-coat dewetting, resulting in extremely straight alignment ($\psi > 0.975$) along the dewetting direction. According to the threshold shear rate of BCP alignment from Nikoubashman et al.,[37] our dewetting-induced shear alignment are above the threshold condition at all temperatures. However, because our dewetting-induced shear is not actually a steady shear but rather a one-time, tsunami-like process, the rest of the annealing time (2 h) is devoted to defect annihilation and morphological improvement of sheared microdomains. This explains why the films treated at higher temperatures have straighter and more ordered microdomains. Further increases in annealing temperature lead, however, to poorer alignment. At 200 °C indeed, which is already over the melting temperature of partially hydrolyzed PVA, the PVA liquid simultaneously migrates on entire BCP film, leading to spinodal decomposition. This reduced microscale directionality of the flow results in a lower degree of directional alignment of the BCP microdomains compared with the situation at 160 °C or 180 °C.

The hole size and dewetting velocity can be controlled by varying the top coat thickness without altering the BCP film conditions. The hole diameter, dewetting velocity, and the degree of alignment of BCP microdomains in PVA/BCP (150 nm thick) bilayer films with 50–500 nm thick top coats are shown in **Figure 5** after thermal annealing at 180 °C. Optical and SEM images showing the appearance and microdomain alignment of these samples are presented in Figures S2 and S3, Supporting Information. With thicker top coats, surface undulation and instability of top coat are difficult to initiate the nucleation of dewetting, leading to larger dewetting holes and longer directional alignment of the BCP microdomains, up to 250 μm with a 500 nm-thick top coat. Also, the dewetting velocity decreases gradually, from ≈370 nm s^{-1} to ≈40 nm s^{-1}, because the very low viscosity of PVA at 180 °C leads to inertial dewetting regime.[39] However, the alignment of the BCP microdomains remains substantial ($\psi > 0.95$) for all top-coat thicknesses, with shear rates ranging from 3.3 s^{-1} to 0.33 s^{-1}. The orientational order parameter increases slightly from 50 nm to 200 nm thickness, and decreases thereafter. We surmise that the rim width, which is equivalent to the effective shearing region, is slightly too narrow with the thinner top coats for perfectly aligned BCP microdomains, while the low shear rates could explain the marginal decrease in alignment measured for the thicker films.

To investigate whether patterns other than sunburst-type alignment could be obtained, a micropatterned top coat was used to control the dewetting direction and thereby the directionality of microdomain alignment. **Figure 6**a illustrates the top coat micropattern imprinting process used to align the BCP microdomains in a single direction. First, we imprinted the PVA/BCP bilayer films with 80 μm/30 μm line-space pattern molds by thermal imprinting at 100 °C and 2 MPa for a 40 min.

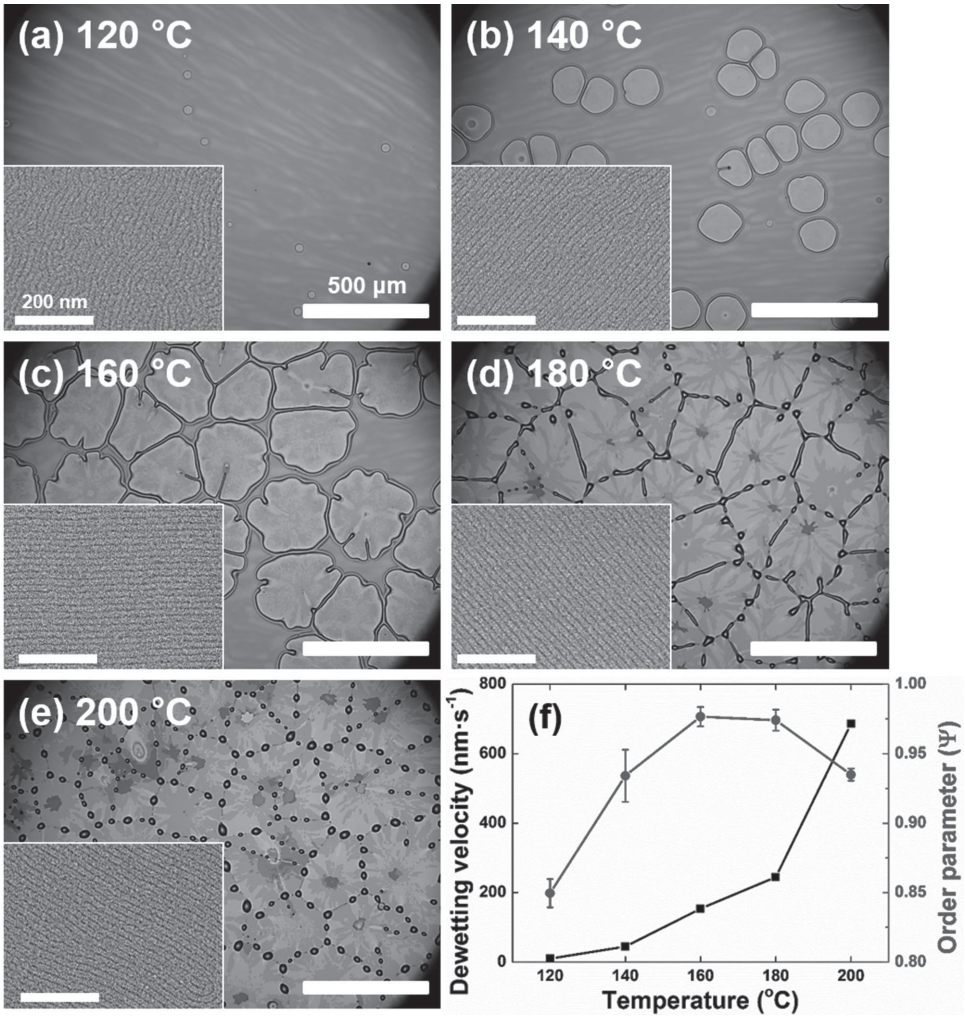

Figure 4. Optical and (inset) scanning electron images of 300 nm-thick top coats on 150 nm-thick block copolymer films annealed at a) 120 °C, b) 140 °C, c) 160 °C, d) 180 °C, and e) 200 °C for 2 h. f) Average velocity of the dewetting top front and orientational order parameter of the block copolymer films as a function of the annealing temperature.

Topographical patterns are formed on the imprinted top coat/BCP, as shown in Figure 6b. During thermal annealing at 180 °C, dewetting occurs in the trenches with the dewetting front moving unidirectionally toward the edges of the pattern (Figure 6c). Thereby, the BCP microdomains in the dewetted area exhibit unidirectional and extremely straight alignment perpendicular to the line-space micropatterns. As can be seen in Figure 6d–f, highly ordered ($\psi \geq 0.99$) and unidirectional alignment (the color maps are identical) is confirmed in three different locations 30 μm apart in the dewetted trench. These results therefore indicate that this patterned top coat affords direction-controlled dewetting in specific microscale areas, and can therefore be used to prepare complex and precise sub-10 nm line patterns such as integrated circuits and FinFET structures.

3. Conclusion

In this study, extremely straight and highly ordered 10 nm-wide PS-*b*-PDMS cylindrical microdomains were created in thin films by dewetting the top coat under thermal annealing to engage shear flow in the BCP underlayer. Sunburst-type patterns are formed around the nucleation point and continue to the rim of the dewetted top coat, over a distance of 150 μm and with an aspect ratio of 15 000:1. The microdomain morphologies were investigated first, as a function of BCP film thickness to better understand the surface/interface effect; second, as a function of annealing temperature to study the effect of top coat/BCP mobility; and third, as a function of top coat thickness to evaluate the effect of different shear rate. Highly ordered BCP patterns were obtained for a wide range of shear rates, but other than at the highest temperature (200 °C), the reduced surface/interface effect and high mobility at higher temperatures resulted in improved microdomain ordering. We also devised a micropatterned top-coat system that provides directional dewetting and unidirectional alignment of BCP patterns in specific areas. This approach—facilitated by the use of sub-10 nm-diameter low molecular weight BCPs—allows the facile deposition of complex directional nanopatterns and can be applied to the directed self-assembly of next-generation sub-7 nm semiconductors and FinFET structures.

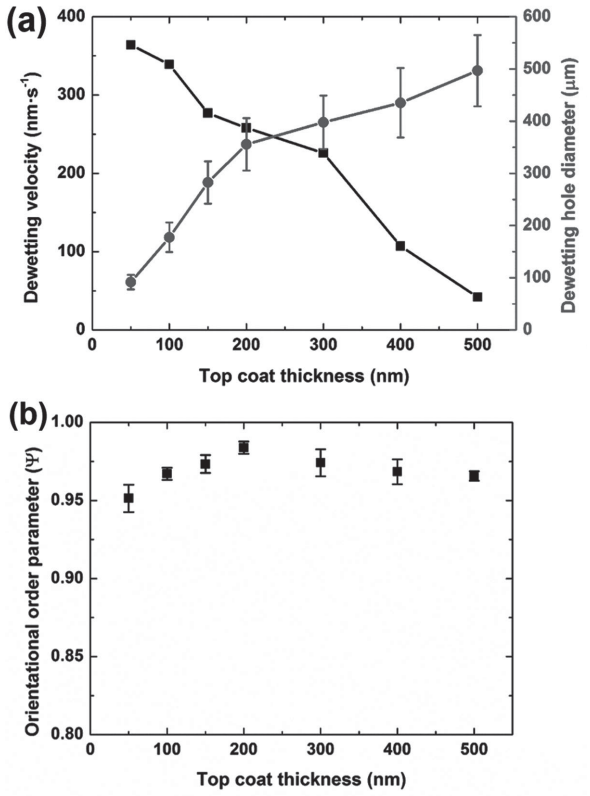

Figure 5. a) Average velocity of the dewetting top front and the average hole diameter in the top coat as a function of top-coat thickness for block copolymer films dewetted at 180 °C. b) Orientational order parameters of the microdomains in 150 nm-thick block copolymer films as a function of top-coat thickness.

4. Experimental Section

Preparation of Block Copolymer/Top Coat Bilayer: Polystyrene-*block*-poly(dimethylsiloxane) (M_w ≈11-*b*-5 kg mol^{-1}, PDI ≈1.08) purchased from Polymersource, Inc. and 40% hydrolyzed polyvinyl alcohol (M_w ≈72 kg mol^{-1}), which contains 60% unhydrolyzed polyvinyl acetate (PVAc), was purchased from Polyscience, Inc. and used as the top coat material. 1–7 wt% of PS-*b*-PDMS solution in cyclohexane was spin-coated at 4000 rpm onto UV/Ozone cleaned Si wafer. The BCP films were dried in vacuum at 60 °C for 2 h. Then 1–10 wt% of PVA solution in methanol was spin-coated again at 8000 rpm onto previously deposited BCP films. The bilayer films were dried again in vacuum oven at room temperature for 2 h.

Top Coat Dewetting and Imaging: To occur the dewetting of top coat, the bilayer films were thermally annealed in vacuum oven for 2 h from 120 to 200 °C. When we measured the velocity of dewetting front, the films were annealed at nitrogen atmosphere for in situ optical observation. The morphology of dewetted films were first observed using optical microscope (Nikon, Eclipse E400POL), then the films were immersed and rinsed with methanol to remove dewetted PVA top coat. To observe the alignment of BCP microdomains more easily, the films were etched and formed topographical patterns with 3 s of CF_4 (50 W, 15 sccm) and subsequent 20 s of O_2 (90 W, 10 sccm) reactive ion etching (RIE) process. The obtained topographical BCP patterns were microscopically examined using field emission-scanning electron microscopy (FE-SEM, JEOL LSM-6701F). The orientational color maps and order parameters were obtained from the image analysis (OrientationJ, macro plug-in of ImageJ) based on at least five SEM images.

Directional Dewetting with Imprinting: We first made PDMS mold from 80 μm mesa and 30 μm trench line-space template patterns with 15 μm step-height. The PDMS prepolymer (Dow corning corporation, SYLGARD 184) were poured to template patterns and cured at 60 °C in vacuum condition for 12 h. The transferred PDMS pattern was used as an imprinting mold. The imprinting was executed at 2 MPa and 100 °C for 40 min with manmade imprinting machine. The patterned bilayer films were thermal annealed with previously described condition for the directional dewetting.

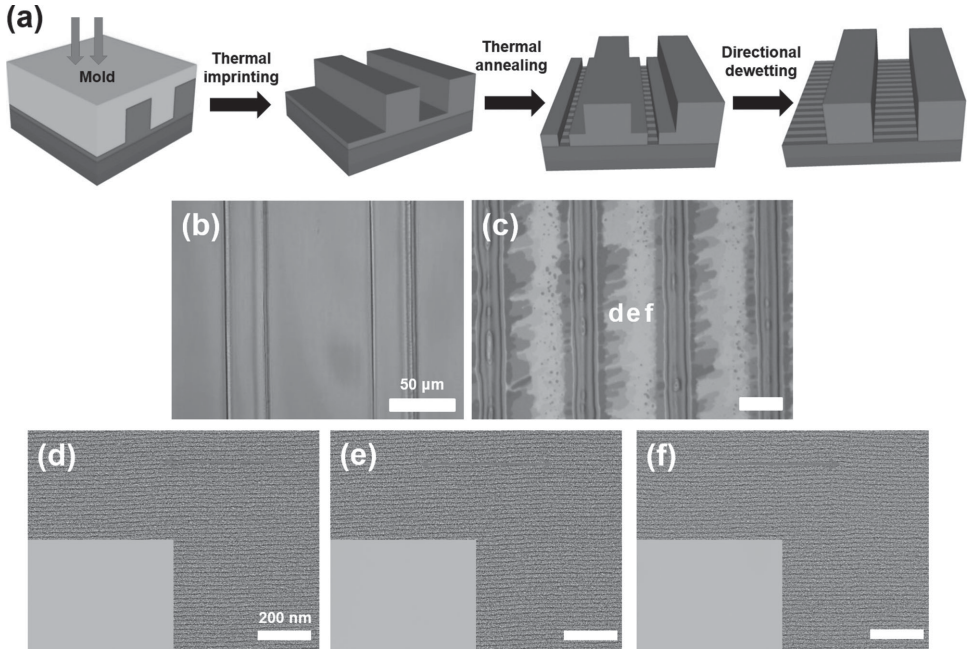

Figure 6. a) Schematic diagram highlighting top-coat micropattern-induced directional dewetting and the resulting alignment of block copolymer microdomains in a specific area. Optical images of imprinted double layer top coat/block copolymer films b) before and c) after dewetting. d–f) Scanning electron images and (inset) the corresponding orientational color maps of block copolymer microdomains obtained in the dewetted regions marked in c).

Supporting Information

Supporting Information is available from the Wiley Online Library or from the author.

Acknowledgements

The authors gratefully acknowledge financial support from the Global Frontier Research Program (2011-0032156) funded by the Korean Government (MEST) and Korea Institute of Science and Technology (KIST) internal project (2E24821). The present research was also conducted by a research grant of the Kwangwoon University in 2014.

Received: September 4, 2014
Revised: November 26, 2014
Published online: December 18, 2014

[1] F. S. Bates, G. H. Fredrickson, *Annu. Rev. Phys. Chem.* **1990**, *41*, 525.
[2] H.-C. Kim, S.-M. Park, W. D. Hinsberg, *Chem. Rev.* **2010**, *110*, 146.
[3] M. Park, C. Harrison, P. M. Chaikin, R. A. Register, D. H. Adamson, *Science* **1997**, *276*, 1401.
[4] J. Y. Cheng, C. A. Ross, H. I. Smith, E. L. Thomas, *Adv. Mater.* **2006**, *18*, 2505.
[5] M. Lazzari, M. A. López-Quintela, *Adv. Mater.* **2003**, *15*, 1583.
[6] J. Bang, U. Jeong, D. Y. Ryu, T. P. Russell, C. J. Hawker, *Adv. Mater.* **2009**, *21*, 4769.
[7] J. Y. Cheng, C. A. Ross, E. L. Thomas, H. I. Smith, G. J. Vancso, *Adv. Mater.* **2003**, *15*, 1599.
[8] R. A. Segalman, H. Yokoyama, E. J. Kramer, *Adv. Mater.* **2001**, *13*, 1152.
[9] Y. S. Jung, C. A. Ross, *Nano Lett.* **2007**, *7*, 2046.
[10] S.-J. Jeong, J. E. Kim, H.-S. Moon, B. H. Kim, S. M. Kim, J. B. Kim, S. O. Kim, *Nano Lett.* **2009**, *9*, 2300.
[11] S. Jeong, H. Moon, B. H. Kim, J. Y. Kim, J. Yu, S. Lee, M. G. Lee, H. Choi, S. O. Kim, *ACS Nano* **2010**, *4*, 5181.
[12] J. G. Son, A. F. Hannon, K. W. Gotrik, A. Alexander-Katz, C. A. Ross, *Adv. Mater.* **2011**, *23*, 634.
[13] I. Bita, J. K. W. Yang, Y. S. Jung, C. A. Ross, E. L. Thomas, K. K. Berggren, *Science* **2008**, *321*, 939.
[14] J. K. W. Yang, Y. S. Jung, J.-B. Chang, R. A. Mickiewicz, A. Alexander-Katz, C. A. Ross, K. K. Berggren, *Nat. Nanotechnol.* **2010**, *5*, 256.
[15] M. P. Stoykovich, M. Müller, S. O. Kim, H. H. Solak, E. W. Edwards, J. J. de Pablo, P. F. Nealey, *Science* **2005**, *308*, 1442.
[16] M. P. Stoykovich, H. Kang, K. C. Daoulas, G. Liu, C. Liu, J. J. De Pablo, M. Müller, P. F. Nealey, *ACS Nano* **2007**, *1*, 168.
[17] S. O. Kim, H. H. Solak, M. P. Stoykovich, N. J. Ferrier, J. J. De Pablo, P. F. Nealey, *Nature* **2003**, *424*, 411.
[18] International Technology Roadmap for Semiconductors (ITRS), **2013**.
[19] B. H. Kim, H. M. Lee, J.-H. Lee, S.-W. Son, S.-J. Jeong, S. Lee, D. Il Lee, S. U. Kwak, H. Jeong, H. Shin, J.-B. Yoon, O. D. Lavrentovich, S. O. Kim, *Adv. Funct. Mater.* **2009**, *19*, 2584.
[20] S. Woo, J. Huh, X. Gu, D. Hyun, W. Ho, S. Park, T. Xu, T. P. Russell, *Proc. Natl. Acad. Sci. USA* **2012**, *109*, 1402.
[21] P. W. Majewski, M. Gopinadhan, C. O. Osuji, *J. Polym. Sci., Part B: Polym. Phys.* **2012**, *50*, 2.
[22] M. Gopinadhan, P. Majewski, Y. Choo, C. Osuji, *Phys. Rev. Lett.* **2013**, *110*, 078301.
[23] A. Keller, E. Pedemonte, F. M. Willmouth, *Nature* **1970**, *225*, 538.
[24] M. A. Villar, D. R. Rueda, F. Ania, E. L. Thomas, *Polymer* **2002**, *43*, 5139.
[25] D. E. Angelescu, J. H. Waller, D. H. Adamson, P. Deshpande, S. Y. Chou, R. A. Register, P. M. Chaikin, *Adv. Mater.* **2004**, *16*, 1736.
[26] G. Singh, K. G. Yager, B. Berry, H.-C. Kim, A. Karim, *ACS Nano* **2012**, *6*, 10335.
[27] V. Pelletier, D. H. Adamson, R. A. Register, P. M. Chaikin, *Appl. Phys. Lett.* **2007**, *90*, 163105.
[28] Z. Qiang, Y. Zhang, J. A. Groff, K. A. Cavicchi, B. D. Vogt, *Soft Matter* **2014**, *10*, 6068.
[29] Z. Qiang, L. Zhang, G. E. Stein, K. A. Cavicchi, B. D. Vogt, *Macromolecules* **2014**, *47*, 1109.
[30] C. M. Bates, T. Seshimo, M. J. Maher, W. J. Durand, J. D. Cushen, L. M. Dean, G. Blachut, C. J. Ellison, C. G. Willson, *Science* **2012**, *338*, 775.
[31] M. J. Maher, C. M. Bates, G. Blachut, S. Sirard, J. L. Self, M. C. Carlson, L. M. Dean, J. D. Cushen, W. J. Durand, C. O. Hayes, C. J. Ellison, C. G. Willson, *Chem. Mater.* **2014**, *26*, 1471.
[32] A. Ramírez-Hernández, H. S. Suh, P. F. Nealey, J. J. de Pablo, *Macromolecules* **2014**, *47*, 3520.
[33] E. Kim, W. Kim, K. H. Lee, C. A. Ross, J. G. Son, *Adv. Funct. Mater.* **2014**, *24*, 6981.
[34] F. B. Wyart, P. Martin, C. Redon, *Langmuir* **1993**, *9*, 3682.
[35] R. J. Andrews, E. A. Grulke, in *Polymer Handbook* (Eds: J. Brandrup, E. H. Immergut, E. A. Grulke, A. Abe, D. R. Bloch), 4th Ed., Wiley, New York, **1999**, pp. VI/193–253.
[36] S. Pujari, M. A. Keaton, P. M. Chaikin, R. A. Register, *Soft Matter* **2012**, *8*, 5358.
[37] A. Nikoubashman, R. L. Davis, B. T. Michal, P. M. Chaikin, R. A. Register, A. Z. Panagiotopoulos, *ACS Nano* **2014**, *8*, 8015.
[38] C. Harrison, P. M. Chaikin, D. A. Huse, R. A. Register, D. H. Adamson, A. Daniel, E. Huang, P. Mansky, T. P. Russell, C. J. Hawker, D. A. Egolf, I. V. Melnikov, E. Bodenschatz, *Macromolecules* **2000**, *33*, 857.
[39] N. Péron, F. Brochard-Wyart, H. Duval, *Langmuir* **2012**, *28*, 15844.